Measurement of the energy spectra of proton, helium and boron cosmic-rays with CALET on the International Space Station

XII International Conference on New Frontieres in Physics

Sandro Gonzi[1,2,3] for the **CALET Collaboration**

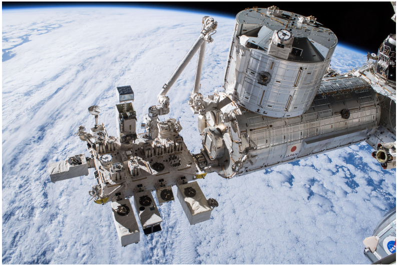

1. University of Florence, Department of Physics and Astronomy, Italy

2. National Institute for Nuclear Physics INFN, Division of Florence, Italy

3. National Research Council CNR, Institute of Applied Physics IFAC, Italy

Table of contents

Table of contents

The CALET mission

The **CALorimetric Electron Telescope (CALET)**, operating aboard the **International Space Station (ISS)** since October 2015, is an experiment dedicated to high-energy astroparticle physics.

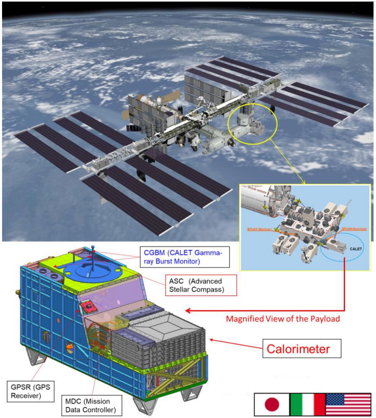

Figure 1: The CALET mission on the ISS.

Remarkable events:

- August 19th, 2015: launched by the Japanese H2-B rocket;
- August 25th, 2015: emplaced on JEM-EF (Japanese Experiment Module Exposed Facility) port #9;
- October 13th, 2015: start of stable observations, more than 2.7 billion events collected so far.

CALET payload

- **Mass** 612.8 kg (JEM Standard Payload)
- **Size**: 1850 mm(L) × 800 mm(W) × 1000 mm(H)
- **Power**: 507 W (max)
- **Telemetry**: Medium 600 kbps (6.5 GB/day)

CALET observations and physics targets

Overview of CALET observations:

- direct cosmic-ray observations in space at the highest energy region by combining:
  - √ a large-size detector;
  - √ long-term observation onboard the ISS;
- electron observation in the 1 GeV - 20 TeV energy range, with high energy resolution;
  - ⇒ search for dark matter and nearby cosmic-ray sources;
- observation of cosmic-ray nuclei in the 10 GeV - 1 PeV energy range;
  - ⇒ unravelling the cosmic-ray acceleration and propagation mechanism;
- detection of transients in space by long-term stable observations:
  - ⇒ electromagnetic radiation from gravitational wave sources, gamma-ray bursts, solar flares, *etc.*

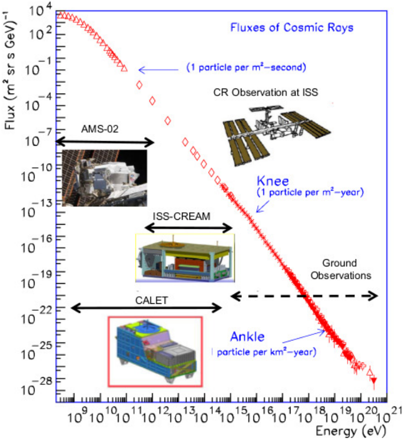

FIGURE 2: cosmic-ray observations on the ISS.

Experiments installed on the ISS

AMS-02, CALET and ISS-CREAM are carrying out complementary measurements.

The CALET detector

CALET detector [1] employs a **calorimeter** with a field of view of $\sim 45^\circ$ from zenith, a geometrical factor of ~ 1040 cm^2 sr and a total depth of ~ 30 radiation-length X_0 for particles at normal incidence.

It consists of:

- **CHarge Detector (CHD)**: a pair of plastic scintillator hodoscopes arranged in two orthogonal layers, in order to identify the charge of the incident particle;
- **IMaging Calorimeter (IMC)**: a sampling calorimeter made of alternated thin layers of Tungsten absorber and scintillating fibers read-out individually;
- **Total AbSorption Calorimeter (TASC)**: a packed lead-tungstate (PWO) hodoscope, capable of almost complete containment of the TeV-electromagnetic showers.

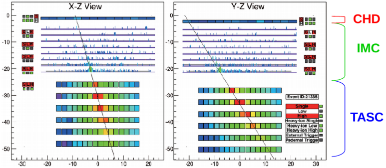

FIGURE 3: electron (or positron) event candidate (reconstructed energy of 3.05 TeV and energy deposit sum of 2.89 TeV).

This design leads to excellent **detector performances**: an electromagnetic shower energy resolution of $\sim 2\%$ above 20 GeV and a protons rejection factor of $\sim 10^5$.

[1] S. Torii, P. S. Marrocchesi *et al.*, *Adv. Space Res.*, **64** (2019) 2531

The CALET instrumentation

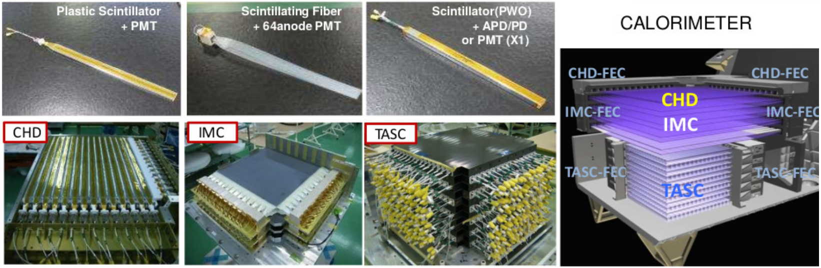

FIGURE 4: overview of the CALET instrumentation.

	CHD (CHarge Detector	IMC (IMaging Calorimeter)	TASC (Total AbSorption Calorimeter)
Measure	Charge (Z=1-40)	Tracking, Particle ID	Energy, e/p Separation
Geometry (Material)	Plastic Scintillator 14 paddles $\times$ 2 layers (X,Y): 28 paddles Paddle Size: $(32 \times 10 \times 450)$ mm^3	448 SciFi $\times$ 16 layers (X,Y) : 7168 SciFi 7 W layers (3 X_0): $0.2 \cdot X_0 \times 5 + 1 \cdot X_0 \times 2$ SciFi size : $(1 \times 1 \times 448)$ mm^3	16 PWO logs $\times$ 12 layers (X,Y): 192 logs log size: $(19 \times 20 \times 326)$ mm^3 Total Thickness: 27 X_0, $\sim$ 1.2 λ_I
Readout	PMT + CSA	64-anode PMT + ASIC	APD/PD + CSA PMT + CSA (for Trigger) @ top layer

Total thickness

The total thickness of the instrument is equivalent to **30 X_0** and **1.3 λ_I**.

Table of contents

Data analysis

Motivations:

- observation of spectral features departing from a single power law in the energy spectra of nuclei and different energy dependence of primary and secondary
  - ⇒ investigation of cosmic-ray sources, acceleration model, and propagation effects;
- direct measurement of the fluxes up to several tens of TeV/n
  - ⇒ important information for studying the connection between direct and indirect measurements and extracting information on the origin of the *knee* in the all-particle energy spectrum.

Event selections:

- selections concerning trigger, geometrical acceptance, quality of the reconstructed tracks, charge identification and so on are applied in order to reject the background.

MC simulation:

- MC simulations of the instrument were developed with the EPICS [2] framework;
- digitization of signals and trigger were accurately modelled in simulation and tuned by using beam test results and flight data;
- MC is used to estimate tracking and selection efficiencies and energy unfolding.

[2] K. Kasahara, *Proc. of 24th ICRC*, **1**, 399 (1995)

Table of contents

Proton spectrum

Spectrum measured [3] in
50 GeV $< E <$ 60 TeV

$$\Phi(E) = \frac{N(E)}{\Delta E \; \epsilon(E) \; S\Omega \; T}$$

$\Phi(E)$: proton spectrum
E: proton kinetic energy
$N(E)$: number of events in ΔE bin (after background subtraction)
$S\Omega$: geometrical acceptance (510 cm^2 sr)
T: live time
ΔE: energy bin width
$\epsilon(E)$: total selection efficiency

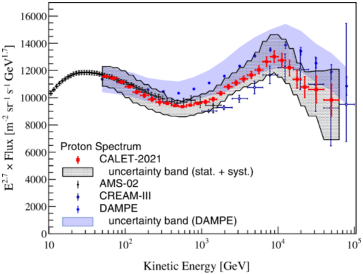

FIGURE 5: cosmic-ray proton spectrum measured by CALET compared with the experimental results of AMS-02, CREAM-III, and DAMPE.

CALET spectrum is in good agreement with:

- rigidity spectra measured by magnetic spectrometers in the sub-TeV region;
- measurements carried out with calorimetric instruments at higher energies.

Observations

The analysis confirms the presence of a spectral **hardening** at a few hundred GeV (significance of more than 20 sigma) and observes a spectral **softening** around 10 TeV.

---

[3] O. Adriani *et al.*, *Phys. Rev. Lett.* **129** (2022) 101102

Fit on the proton spectrum

Proton spectrum is not consistent with a single power law covering the whole range.

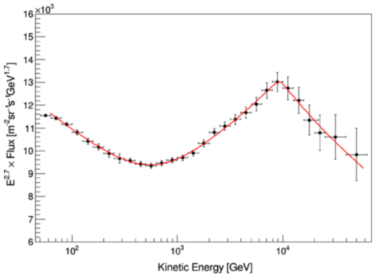

FIGURE 6: CALET proton spectrum fitted with a DBPL function.

DPBL parameter	Fitted value	spectrum region
γ	$-2.83^{+0.01}_{-0.02}$	low energy
$\Delta\gamma$	$0.28^{+0.04}_{-0.02}$	hardening
E_0	584^{+61}_{-58} GeV	hardening
s	$2.4^{+0.8}_{-0.6}$	hardening
$\Delta\gamma_1$	$-0.34^{+0.06}_{-0.06}$	softening
E_1	$9.3^{+1.4}_{-1.1}$ TeV	softening
s_1	~ 30	softening

Proton spectrum fitted in $80\ \mathrm{GeV} < E < 60\ \mathrm{TeV}$ with a **double broken power law (DBPL)**:

$$\Phi(E) = C\left(\frac{E}{1\ GeV}\right)^{\gamma}\left[1+\left(\frac{E}{E_0}\right)^{s}\right]^{\frac{\Delta\gamma}{s}}\left[1+\left(\frac{E}{E_1}\right)^{s_1}\right]^{\frac{\Delta\gamma_1}{s_1}}$$

A gradual hardening is followed by a sharp softening at about 9 TeV ($s_1 >> s$, large uncertainty). Spectrum shape is consistent with the most recent results of DAMPE.

Table of contents

Helium spectrum

Spectrum measured [4] in
40 GeV $< E <$ 250 TeV

$$\Phi(E) = \frac{N(E)}{\Delta E \; \epsilon(E) \; S\Omega \; T}$$

$\Phi(E)$: helium spectrum
E: helium kinetic energy
$N(E)$: number of events in ΔE bin (after background subtraction)
$S\Omega$: geometrical acceptance (510 cm^2 sr)
T: live time
ΔE: energy bin width
$\epsilon(E)$: total selection efficiency

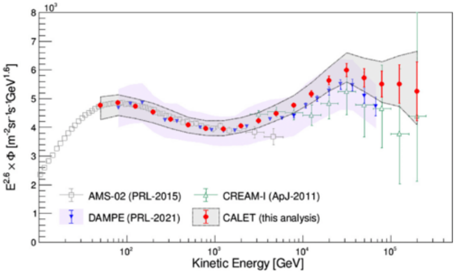

FIGURE 7: cosmic-ray helium spectrum measured by CALET compared with the experimental results of AMS-02, CREAM-I, and DAMPE.

CALET spectrum is in good agreement with:

- rigidity spectra measured by magnetic spectrometers in the sub-TeV region;
- measurements carried out with calorimetric instruments at higher energies.

Observations

The analysis observes a spectral **hardening** from a few hundred GeV to a few tens TeV and also observes the onset of a spectral **softening** above a few tens of TeV.

[4] O. Adriani *et al.*, *Phys. Rev. Lett.* **130** (2023) 171002

Fit on the helium spectrum

Helium spectrum is not consistent with a single power law covering the whole range.

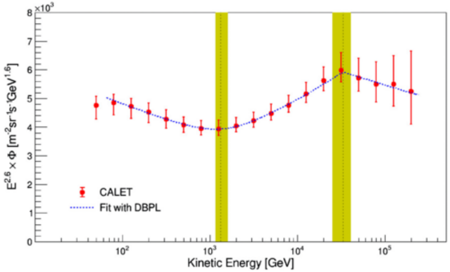

FIGURE 8: CALET helium spectrum fitted with a DBPL function.

DPBL parameter	Fitted value	spectrum region
γ	$-2.703^{+0.005}_{-0.006}(\text{stat})^{+0.032}_{-0.009}(\text{syst})$	low energy
$\Delta\gamma$	$0.25^{+0.02}_{-0.01}(\text{stat})^{+0.02}_{-0.03}(\text{syst})$	hardening
E_0	$1319^{+113}_{-93}(\text{stat})^{+267}_{-124}(\text{syst})$ GeV	hardening
s	$2.7^{+0.6}_{-0.5}(\text{stat})^{+3.0}_{-0.9}(\text{syst})$	hardening
$\Delta\gamma_1$	$-0.22^{+0.07}_{-0.10}(\text{stat})^{+0.03}_{-0.04}(\text{syst})$	softening
E_1	$33.2^{+9.8}_{-6.2}(\text{stat})^{+1.8}_{-2.3}(\text{syst})$ TeV	softening
s_1	~ 30	softening

Spectrum fitted in 60 GeV $< E <$ 250 TeV with a **double broken power law (DBPL)**:

$$\Phi(E) = C\left(\frac{E}{1\ GeV}\right)^{\gamma}\left[1+\left(\frac{E}{E_0}\right)^{s}\right]^{\frac{\Delta\gamma}{s}}\left[1+\left(\frac{E}{E_1}\right)^{s_1}\right]^{\frac{\Delta\gamma_1}{s_1}}$$

The index change $\Delta\gamma$ is proven to be different from zero by more than 8 sigma. DBPL fit parameters are consistent, within the errors, with the most recent results of DAMPE.

p/He flux ratio

Differences between the proton and helium spectra provide important constraints on acceleration models.

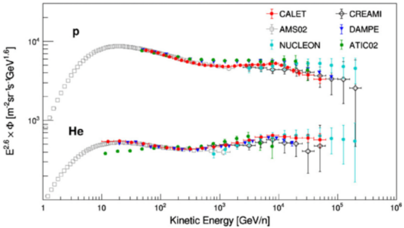

FIGURE 9: CALET proton and helium fluxes, as a functions of kinetic energy per nucleon, compared with other direct measurements.

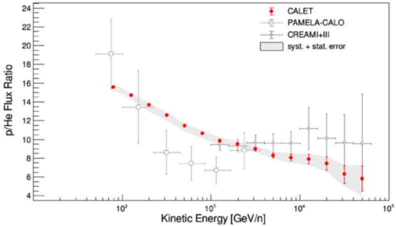

FIGURE 10: energy spectrum of p/He ratio measured by CALET compared with the experimental results of CREAM and PAMELA.

The p/He flux ratio has been measured in 60 $\mathrm{GeV}/n < E < 60\ \mathrm{TeV}/n$.

CALET results are in agreement with previous measurements from magnetic spectrometers up to their maximum detectable rigidity ($\sim$ 2 TV) and extend the measurements at high energy, with high precision.

Table of contents

Boron and carbon spectra

Spectrum measured [5] in
$8.4\ \mathrm{GeV}/n < E < 3.8\ \mathrm{TeV}/n$

$$\Phi(E) = \frac{N(E)}{\Delta E\ \epsilon(E)\ S\Omega\ T}$$

$\Phi(E)$: boron or carbon spectrum
E: boron or carbon kinetic energy per nucleon
$N(E)$: number of events in ΔE bin (after background subtraction)
$S\Omega$: geometrical acceptance (510 cm^2 sr)
T: live time
ΔE: energy bin width
$\epsilon(E)$: total selection efficiency

We observe that:

- the B spectrum is consistent with PAMELA but the absolute normalization is in tension with AMS-02 (as for C, O, and Fe measured fluxes);
- the B/C ratio is consistent with AMS-02.

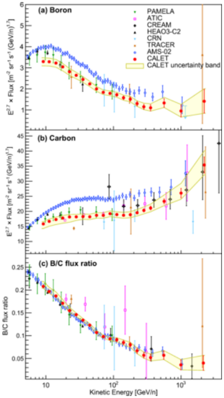

FIGURE 11: (a) boron (b) carbon and (c) ratio of boron to carbon spectra measured by CALET compared with other direct measurements.

Observations

The analysis confirms (for carbon) and observes (for boron) the presence of a spectral **hardening** at a few hundred GeV.

[5] O. Adriani *et al.*, *Phys. Rev. Lett.* **129** (2022) 251103

Fit on the boron and carbon spectra

Boron and carbon spectra are not consistent with a single power law in the whole range.

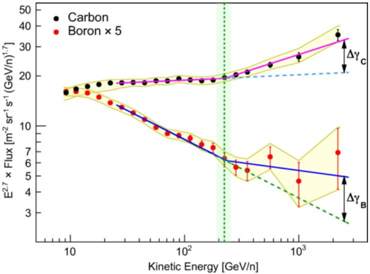

FIGURE 12: CALET B and C energy spectra fitted with DPL functions.

For carbon:

DPL parameter	Fitted value	spectrum region
γ^C	-2.670 ± 0.005	low energy
$\Delta\gamma^C$	0.19 ± 0.03	hardening
E_0^C	(220 ± 20) GeV$/n$	hardening

For boron:

DPL parameter	Fitted value	spectrum region
γ^B	-3.047 ± 0.024	low energy
$\Delta\gamma^B$	0.25 ± 0.12	hardening
E_0^B	220 GeV$/n$ (fixed)	hardening

Spectrum fitted in 25 GeV $< E <$ 3.8 TeV with a **double power law (DPL)**:

$$\Phi(E) = \begin{cases} C\left(\frac{E}{1\ \mathrm{GeV}}\right)^{\gamma} & E \leq E_0 \\ C\left(\frac{E}{1\ \mathrm{GeV}}\right)^{\gamma}\left(\frac{E}{E_0}\right)^{\Delta\gamma} & E > E_0 \end{cases}$$

The energy spectra are different as expected for primary and secondary cosmic-rays. The flux hardens more for B than for C, above 200 GeV$/n$.

B/C flux ratio

B/C flux ratio can give informations about the particle transport in the Galaxy.

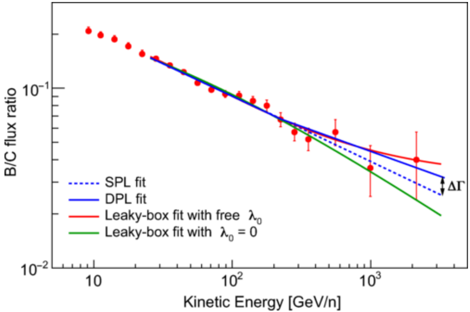

FIGURE 13: The CALET B/C ratio fitted to different functions.

DPL parameter	Fitted value	spectrum region
$\Gamma^{B/C}$	-0.366 ± 0.018	low energy
$\Delta\Gamma^{B/C}$	0.09 ± 0.05	hardening
$E_0^{B/C}$	$220\ \mathrm{GeV}/n$ (fixed)	hardening

Spectrum fitted in $25\ \mathrm{GeV} < E < 3.8\ \mathrm{TeV}$ with a **double power law (DPL)**:

This result is consistent with that of AMS-02 and supports the hypothesis that secondary B exhibits a stronger hardening than primary C.

No definitive conclusion can be drawn due to the large uncertainty in $\Delta\Gamma^{B/C}$ given by our present statistics.

Conclusions

CALET was successfully launched on August 19th, 2015, and is successfully carrying out observations since October 2015 with stable instrument performance

Measured light nuclei spectra presented (from few tens of GeV up to tens of TeV):

- the **proton** spectrum has been published in PRL 129, 101102 (2022): we observed a spectral hardening and a softening, fitted together with a DBPL;
- the **helium** spectrum has been published in PRL 130, 171002 (2023): we observed a spectral hardening and the onset of a softening, fitted together with a DBPL;
- the **boron** and **carbon** spectra have been published in PRL 129, 251103 (2022): we observed a spectral hardening at about the same energy per nucleon, fitted both with a DPL;

Measured flux ratio presented (information on acceleration and propagation models):

- **p**/**He** flux ratio;
- **B**/**C** flux ratio: fitted with a DPL.

Further observations will improve the measurement of nuclei spectra by better statistics and a further reduction of the systematic errors, especially in the TeV region.

Thank you
for your attention

We gratefully acknowledge JAXA's contributions to the development of CALET and to the operations onboard the International Space Station. The CALET effort in Italy is supported by ASI under Agreement No. 2013- 018-R.0 and its amendments. The CALET effort in the United States is supported by NASA through Grants No. 80NSSC20K0397, No. 80NSSC20K0399, and No. NNH18ZDA001N-APRA18-0004. This work is supported in part by JSPS Grant-in- Aid for Scientific Research (S) Grant No. 19H05608 in Japan.

Backup slides

Full Authors List: CALET Collaboration

O. Adriani[1,2], Y. Akaike[3,4], K. Asano[5], Y. Asaoka[5], E. Berti[2,6], G. Bigongiari[7,8], W.R. Binns[9], M. Bongi[1,2], P. Brogi[7,8], A. Bruno[10], N. Cannady[11,12,13], G. Castellini[6], C. Checchia[7,8], M.L. Cherry[14], G. Collazuol[15,16], G.A. de Nolfo[10], K. Ebisawa[17], A.W. Ficklin[14], H. Fuke[17], S. Gonzi[1,2,6], T.G. Guzik[14], T. Hams[11], K. Hibino[18], M. Ichimura[19], K. Ioka[20], W. Ishizaki[5], M.H. Israel[9], K. Kasahara[21], J. Kataoka[22], R. Kataoka[23], Y. Katayose[24], C. Kato[25], N. Kawanaka[20], Y. Kawakubo[14], K. Kobayashi[3,4], K. Kohri[26], H.S. Krawczynski[9], J.F. Krizmanic[12], P. Maestro[7,8], P.S. Marrocchesi[7,8], A.M. Messineo[8,27], J.W. Mitchell[12], S. Miyake[28], A.A. Moiseev[29,12,13], M. Mori[30], N. Mori[2], H.M. Motz[18], K. Munakata[25], S. Nakahira[17], J. Nishimura[17], S. Okuno[18], J.F. Ormes[31], S. Ozawa[32], L. Pacini[2,6], P. Papini[2], B.F. Rauch[9], S.B. Ricciarini[2,6], K. Sakai[11,12,13], T. Sakamoto[33], M. Sasaki[29,12,13], Y. Shimizu[18], A. Shiomi[34], P. Spillantini[1], F. Stolzi[7,8], S. Sugita[33], A. Sulaj[7,8], M. Takita[5], T. Tamura[18], T. Terasawa[5], S. Torii[3], Y. Tsunesada[35,36], Y. Uchihori[37], E. Vannuccini[2], J.P. Wefel[14], K. Yamaoka[38], S. Yanagita[39], A. Yoshida[33], K. Yoshida[21], and W.V. Zober[9]

[1]Department of Physics, University of Florence, Via Sansone, 1 - 50019, Sesto Fiorentino, Italy, [2]INFN Sezione di Firenze, Via Sansone, 1 - 50019, Sesto Fiorentino, Italy, [3]Waseda Research Institute for Science and Engineering, Waseda University, 17 Kikuicho, Shinjuku, Tokyo 162-0044, Japan, [4]JEM Utilization Center, Human Spaceflight Technology Directorate, Japan Aerospace Exploration Agency, 2-1-1 Sengen, Tsukuba, Ibaraki 305-8505, Japan, [5]Institute for Cosmic Ray Research, The University of Tokyo, 5-1-5 Kashiwa-no-Ha, Kashiwa, Chiba 277-8582, Japan, [6]Institute of Applied Physics (IFAC), National Research Council (CNR), Via Madonna del Piano, 10, 50019, Sesto Fiorentino, Italy, [7]Department of Physical Sciences, Earth and Environment, University of Siena, via Roma 56, 53100 Siena, Italy, [8]INFN Sezione di Pisa, Polo Fibonacci, Largo B. Pontecorvo, 3 - 56127 Pisa, Italy, [9]Department of Physics and McDonnell Center for the Space Sciences, Washington University, One Brookings Drive, St. Louis, Missouri 63130-4899, USA, [10]Heliospheric Physics Laboratory, NASA/GSFC, Greenbelt, Maryland 20771, USA, [11]Center for Space Sciences and Technology, University of Maryland, Baltimore County, 1000 Hilltop Circle, Baltimore, Maryland 21250, USA, [12]Astroparticle Physics Laboratory, NASA/GSFC, Greenbelt, Maryland 20771, USA, [13]Center for Research and Exploration in Space Sciences and Technology, NASA/GSFC, Greenbelt, Maryland 20771, USA, [14]Department of Physics and Astronomy, Louisiana State University, 202 Nicholson Hall, Baton Rouge, Louisiana 70803, USA, [15]Department of Physics and Astronomy, University of Padova, Via Marzolo, 8, 35131 Padova, Italy, [16]INFN Sezione di Padova, Via Marzolo, 8, 35131 Padova, Italy, [17]Institute of Space and Astronautical Science, Japan Aerospace Exploration Agency, 3-1-1 Yoshinodai, Chuo, Sagamihara, Kanagawa 252-5210, Japan, [18]Kanagawa University, 3-27-1 Rokkakubashi, Kanagawa, Yokohama, Kanagawa 221-8686, Japan, [19]Faculty of Science and Technology, Graduate School of Science and Technology, Hirosaki University, 3, Bunkyo, Hirosaki, Aomori 036-8561, Japan, [20]Yukawa Institute for Theoretical Physics, Kyoto University, Kitashirakawa Oiwake-cho, Sakyo-ku, Kyoto, 606-8502, Japan, [21]Department of Electronic Information Systems, Shibaura Institute of Technology, 307 Fukasaku, Minuma, Saitama 337-8570, Japan, [22]School of Advanced Science and Engineering, Waseda University, 3-4-1 Okubo, Shinjuku, Tokyo 169-8555, Japan, [23]National Institute of Polar Research, 10-3, Midori-cho, Tachikawa, Tokyo 190-8518, Japan, [24]Faculty of Engineering, Division of Intelligent Systems Engineering, Yokohama National University, 79-5 Tokiwadai, Hodogaya, Yokohama 240-8501, Japan, [25]Faculty of Science, Shinshu University, 3-1-1 Asahi, Matsumoto, Nagano 390-8621, Japan, [26]Institute of Particle and Nuclear Studies, High Energy Accelerator Research Organization, 1-1 Oho, Tsukuba, Ibaraki, 305-0801, Japan, [27]University of Pisa, Polo Fibonacci, Largo B. Pontecorvo, 3 - 56127 Pisa, Italy, [28]Department of Electrical and Electronic Systems Engineering, National Institute of Technology (KOSEN), Ibaraki College, 866 Nakane, Hitachinaka, Ibaraki 312-8508, Japan, [29]Department of Astronomy, University of Maryland, College Park, Maryland 20742, USA, [30]Department of Physical Sciences, College of Science and Engineering, Ritsumeikan University, Shiga 525-8577, Japan, [31]Department of Physics and Astronomy, University of Denver, Physics Building, Room 211, 2112 East Wesley Avenue, Denver, Colorado 80208-6900, USA, [32]Quantum ICT Advanced Development Center, National Institute of Information and Communications Technology, 4-2-1 Nukui-Kitamachi, Koganei, Tokyo 184-8795, Japan, [33]College of Science and Engineering, Department of Physics and Mathematics, Aoyama Gakuin University, 5-10-1 Fuchinobe, Chuo, Sagamihara, Kanagawa 252-5258, Japan, [34]College of Industrial Technology, Nihon University, 1-2-1 Izumi, Narashino, Chiba 275-8575, Japan, [35]Graduate School of Science, Osaka Metropolitan University, Sugimoto, Sumiyoshi, Osaka 558-8585, Japan, [36]Nambu Yoichiro Institute for Theoretical and Experimental Physics, Osaka Metropolitan University, Sugimoto, Sumiyoshi, Osaka 558-8585, Japan, [37]National Institutes for Quantum and Radiation Science and Technology, 4-9-1 Anagawa, Inage, Chiba 263-8555, Japan, [38]Nagoya University, Furo, Chikusa, Nagoya 464-8601, Japan, [39]College of Science, Ibaraki University, 2-1-1 Bunkyo, Mito, Ibaraki 310-8512, Japan

Proton event selection

1. **offline trigger confirmation**: offline confirmation of the online trigger (High Energy HE in $E > 300$ GeV and Low Energy LE in $E < 300$ GeV);
2. **Geometrical acceptance**: tracks going through the detector from the top to the bottom are selected;
3. **Track quality cut**: reliability of Kalman Filter fitting in IMC is checked;
4. **Electron rejection**: electron events are rejected checking the energy deposit within one Moliere radius along the track;
5. **Rejection of off-acceptance events**: removal of events where a secondary track is identified as the primary track;
6. **TASC hit consistency**: consistency of the track impact point in the TASC with the calorimetric energy deposit;
7. **Shower development in the IMC**: shower development starting in IMC is required;
8. **Charge identification**: identification of the primary particle through the $\frac{dE}{dx}$ measurements in CHD and along the IMC track.

Helium event selection

1. **offline trigger confirmation**: offline confirmation of the online trigger (High Energy HE);
2. **Geometrical acceptance**: tracks going through the detector from the top to the bottom are selected, with 2 cm clearence from the edges of the TASC top layer;
3. **Track quality cut**: reliability of Kalman Filter fitting in IMC is checked;
4. **Electron rejection**: electron events are rejected checking the energy deposit within one Moliere radius along the track;
5. **Rejection of off-acceptance events**: removal of events where a secondary track is identified as the primary track;
6. **TASC hit consistency**: consistency of the track impact point in the TASC with the calorimetric energy deposit;
7. **Shower axis**: the reconstructed shower axis is required to cross the TASC-X1 layer, in order to reject lateral events erroneosly reconstructed in the fiducial region;
8. **Charge identification**: identification of the primary particle through the $\frac{dE}{dx}$ measurements in CHD and along the IMC track.

Boron and Carbon event selection

1. **offline trigger confirmation**: offline confirmation of the online trigger (High Energy HE);
2. **Geometrical acceptance**: tracks going through the detector from the top to the bottom are selected, with 2 cm clearence from the edges of the TASC top layer;
3. **Charge identification**: identification of the primary particle through the $\frac{dE}{dx}$ measurements in CHD and along the IMC track.
4. **Track width**: removal of particle undergoing a charge-changing nuclear interaction in the upper part of the instrument;
5. **Field of View**: removal of the events with the reconstructed events pointing the ISS obstacles in the CALET field of view;

B/C flux ratio

B/C flux ratio was fitted to a DPL and to functions from a leaky-box model describing the particle transport in the Galaxy.

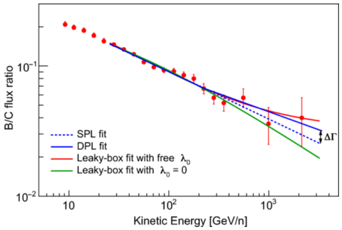

FIGURE 13: The CALET B/C ratio fitted to different functions.

Leaky-Box (LB) model:

$$\frac{\Phi_B(E)}{\Phi_C(E)} = \frac{\lambda(E)\,\lambda_B}{\lambda(E)+\lambda_B}\left[\frac{1}{\lambda_{C\to B}} + \frac{\Phi_O(E)}{\Phi_C(E)}\frac{1}{\lambda_{O\to B}}\right]$$

$$\lambda(E) = kE^{-\delta} + \lambda_0$$

For B/C:

DPL parameter	Fitted value	spectrum region
$\gamma^{B/C}$	-0.366 ± 0.018	low energy
$\Delta\gamma^{B/C}$	0.09 ± 0.05	hardening
$E_0^{B/C}$	220 GeV/n (fixed)	hardening

For Leaky-Box model:

LB parameter	Fitted value
k	(12.0 ± 0.9) g/cm^2
δ	0.71 ± 0.11
λ_0	(0.95 ± 0.35) g/cm^2

λ_B: interaction length of B nuclei with matter of the ISM;
$\lambda_{C\to B}(\lambda_{O\to B})$: average path length for a nucleus C (O) to spall into B;
$\lambda(E)$: mean escape path length;
δ: diffusion coefficient spectral index;
λ_0: residual path length (interpreted as source grammage).

$\lambda_0 \neq 0$ is compatible with the hypothesis that a fraction of secondary B nuclei can be produced near the CR source.